$(H_2O)_6$ on a Virtual Metal Surface: Many-Body Effects in the Bilayer Structure

Timm Lankau*

Institut für Physikalische Chemie, University of Hamburg, 20146 Hamburg, Germany

Received: November 14, 2001; In Final Form: February 26, 2002

Many-body effects in a water hexamer attached to a metal surface have been studied by quantum calculations. The metal component of the interface has been replaced by a set of geometrical constraints (virtual surface) [*J. Phys. Chem. A* **2000**, *105*, 4084−4095] which permits the analysis of the properties of the interface independently of the precise electronic structure of the metal, as a function of the surface lattice constant. Our calculations show that cooperative forces have a significant influence on the energy and geometry of the metal−water interface. The energy decomposition of the energy of formation of the water hexamer demonstrates how strong cooperative effects favor the growth of the water bilayer in the experimentally observed range of surface lattice constants, while a model based solely on two-center energies predicts the formation of the water bilayer at unphysically large values of surface lattice constant.

1. Introduction

The theoretical analysis of the metal−water interface has generated interest recently[1,2] with increasing research into fuel cells. This interface can be observed experimentally either by electrochemical or by UHV (ultra high vacuum) experiments.[3,4] These experiments differ mainly in the number of water molecules involved. UHV experiments allow surface scientists the most direct observation of the first water bilayer at the metal surface, since the observation is not blurred by additional water molecules on top of the first bilayer. An extensive review of the water−metal interaction observed in UHV experiments has been published by Thiel and Madey.[5]

On hexagonal metal surfaces with a surface lattice constant d1 between 2.49 Å (Ni) and 2.89 Å (Ag)[6] (this range is marked in gray in all plots), water can form a structure similar to the $(\sqrt{3} \times \sqrt{3})R\ 30°$ structure observed on Pt(111)[7−11] and Ru(0001).[12−14] Doering and Madey[14] published a modification of the ice rules by Bernal, Fowler, and Pauling[15−17] to describe the structure of water clusters on hexagonal metal surfaces. These rules describe the structure of the bilayer similar to that of the basal plane of ice Ih[18] and assume thereby a seamless transition between the hexagonal metal surface and an ice crystal growing at high water coverage. Specifically,[14] each water molecule is assumed bound by at least two bonds (which may be hydrogen bonds to other water molecules or oxygen lone pair bonds to the surface) while maintaining a tetrahedral bonding configuration. The water molecule is assumed bound to the surface via one lone pair orbital on the oxygen, and all free lone pair orbitals on oxygen stay nearly perpendicular to the surface. In an ideal infinite bilayer, all water molecules have their dipole moments pointing away from the surface, whereas in a finite cluster, water molecules whose dipole moments point toward the surface may occur at the edge of the cluster.[13,14,19]

Weaver et al.[3,4] pointed out the close similarity of the electrochemical and the UHV water interfaces, and the molecular dynamics simulations by Spohr and Heinzinger[20−22] showed a structure similar to the water bilayer observed in UHV experiments. As LEED experiments (low energy electron diffraction) suggest, the cyclic hexamer forms the water bilayer;[5,14] the cyclic hexamer under certain geometrical constraints can therefore be used as model for the water bilayer in UHV and electrochemical experiments.[23]

The free water hexamer in the gas phase delineates two groups of water clusters: clusters with fewer than six water molecules have cyclic equilibrium geometries[24−37] whereas clusters with more than six molecules prefer more compact cage-like structures.[37−49] Several conformers of the hexamer, which marks the border between the two groups of water clusters, are known with similar energies of formation.[35−47,49−67] The most stable water hexamer has a cage-like structure[36,64−73] while the cyclic one marks the upper end of the energy scale. The energy difference between both structures is usually small (≈1 kcal/mol), and the energetic order of all conformers is substantially influenced by multicenter effects within the water clusters. It is interesting to note that two conformers have properties similar to those observed for bulk phases. The hydrogen bonds in the cage-like cluster are similar to those observed in liquid water, while the hydrogen bonds in the cyclic hexamer resemble those of ice Ih,[70] which again demonstrates the close link between the geometries of various water clusters and the structures of liquid water and ice. The close similarity between the cyclic water hexamer and the water bilayer (or ice Ih) was exploited in the analysis of the water bilayer independently of the underlying metal.[23] It was shown that several properties of the water bilayer such as the total energy of formation or the nonplanarity of the ring appear independent of the electronic structure of the metal surface and are controlled purely by the surface lattice constant of the metal. Consequently, many properties of the water bilayer arise from geometrical constraints on the hydrogen bond network within the hexamer.

Just as the properties of the water hexamer conformers,[36,70] as well as the properties of ice[74,75] and liquid water,[76] are strongly influenced by cooperative effects within the hydrogen bond network, the properties of the cyclic water hexamer under surface constraints as a model for the water bilayer are also expected to be controlled by multicenter energies. The analysis of these multicenter energies is the subject of this communication.

* Corresponding author e-mail: lankau@chemie.uni-hamburg.de.

10.1021/jp014206d CCC: $22.00
Published on Web 05/30/2002

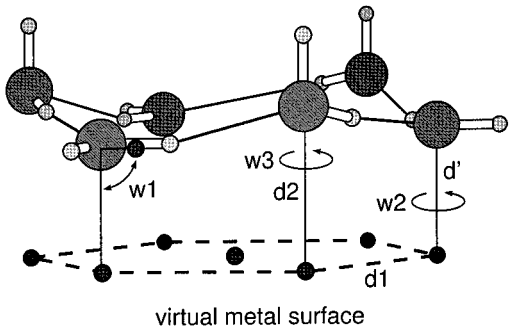

(a) sideview

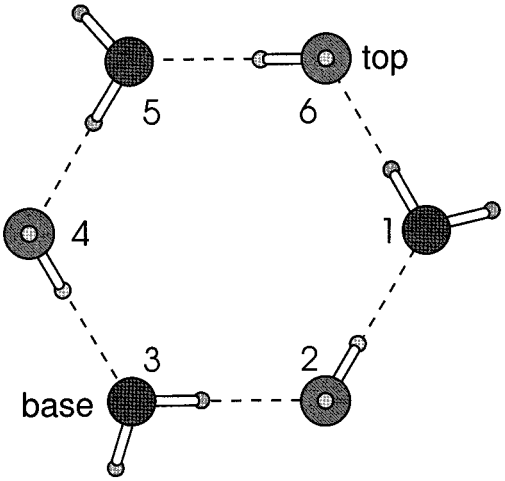

(b) topview

Figure 1. Water hexamer on the virtual surface (d1 = 2.8 Å):[23] (a) side view; (b) top view.

2. Computational Procedure

The structure of the metal−water interface is controlled both by the interaction between surface atoms and the water molecules in the first layer and by the interactions among the water molecules within the bilayer. To distinguish between these two forces the model of the virtual surface[23] was chosen to separate mathematically the water bilayer and the metal surface.

Our model of the metal−water interface used for the calculations reported here was made from two parts: the water bilayer was replaced by a single water hexamer with the same geometry as in the bilayer structure proposed by Doering and Madey[14] while the metal surface was replaced by the virtual one,[23] which is built from a mesh of seven auxiliary geometrical points and a set of geometry constraints acting on the water cluster. Since the auxiliary geometrical points replace the surface atoms and the hexagonal symmetry of the surface was maintained in all calculations, different metals vary only by their value of the surface lattice constant d1, which is defined as the distance between two neighboring auxiliary points (Figure 1a).

The water hexamer is assumed to have the same geometry as a six-membered water ring in an ideal infinite bilayer structure. Each water molecule lies above a virtual metal atom/auxiliary point. The water molecules in the plane closest to the virtual metal surface (basal plane) are assumed to lie at a fixed distance (d′ = 1 Å) from the virtual surface and both hydrogen atoms have the same distance d″ from the surface, which was allowed to vary during geometry optimizations. The geometry of a water molecule in the basal plane attached to an auxiliary geometry point (virtual surface) resembles a Lewis-type water−metal bond via an oxygen lone pair without taking the electronic structure of a real metal surface explicitly into account.

One hydrogen atom of a basal water molecule points away from the ring, while the other is used to form a hydrogen bond to a water molecule in the top plane. In the top plane one hydrogen atom of each water molecule lies perpendicular to the virtual metal surface while the second is used for the hydrogen bond to a water molecule in the basal plane.

Both types of water molecules, basal and top, have two degrees of freedom: a basal water molecule has two rotational degrees (w1 and w2), while a top one has one rotational (w3) and one translational (d2, Figure 1a). The four variables (d2, w1 to w3) were optimized for a given value of the surface lattice constant d1 and the difference d2 − d′ in the optimized water hexamer is a measure for the nonplanarity of the ring. The results of these calculations, which describe the orientation of the water molecules in a bilayer attached to a real metal surface very well, have been reported previously.[23] The optimized geometries from ref 23 were used for the calculation of the multicenter energies in the water hexamer as a function of the surface lattice constant d1 presented in this work.

The method of Hankins et al.,[77] which has been used for the analysis of other water clusters,[34,59−62,78,79] was used to calculate many-body energies in these water hexamers. The absolute energy E_{ABS} of the hexamer ($N = 6$) as a function of the monomer positions ($\mathbf{x}_i$) may be written as the sum of multicenter energies (E_{ic}).

$$E_{ABS}(\mathbf{x}_1, ..., \mathbf{x}_N) = E_{1c} + E_{2c} + E_{3c} + ... + E_{Nc} = \sum_{i=1}^{N} E^{(1)}(\mathbf{x}_i) + \sum_{i<j=1}^{N} V^{(2)}(\mathbf{x}_i, \mathbf{x}_j) + \sum_{i<j<k=1}^{N} V^{(3)}(\mathbf{x}_i, \mathbf{x}_j, \mathbf{x}_k) + ... + V^{(N)}(\mathbf{x}_i, ..., \mathbf{x}_N) \quad (1)$$

In the chosen surface model the single-molecule energies $E^{(1)}(\mathbf{x}_i)$ are equal to the energies of the free monomers E_1, as monomer relaxation was not included in the model. The multicenter energies are given by the sum of the individual multicenter interactions $V^{(i)}(\mathbf{x}_1, ..., \mathbf{x}_i)$ and can be calculated recursively according to the following equation.

$$E^{(1)}(\mathbf{x}_i) \equiv E(\mathbf{x}_i) = E_1$$

$$V^{(2)}(\mathbf{x}_i, \mathbf{x}_j) = E_2(\mathbf{x}_i, \mathbf{x}_j) - E^{(1)}(\mathbf{x}_i) - E^{(1)}(\mathbf{x}_j)$$

$$V^{(3)}(\mathbf{x}_i, \mathbf{x}_j, \mathbf{x}_k) = E_3(\mathbf{x}_i, \mathbf{x}_j, \mathbf{x}_k) - E^{(1)}(\mathbf{x}_i) - E^{(1)}(\mathbf{x}_j) - E^{(1)}(\mathbf{x}_k) - V^{(2)}(\mathbf{x}_i, \mathbf{x}_j) - V^{(2)}(\mathbf{x}_i, \mathbf{x}_k) - V^{(2)}(\mathbf{x}_j, \mathbf{x}_k)$$

$$\vdots \quad (2)$$

To obtain the multicenter interaction energies $V^{(i)}$ the energy ($E_i(\mathbf{x}_1, ..., \mathbf{x}_i)$) of a subset of water molecules is needed. During these calculations the water molecules stay in the same positions ($\mathbf{x}_i$) as in the hexamer.

The necessary cluster energies have been calculated at HF and MP2 levels with Gaussian 94,[80] using Dunning's DZP basis set.[81] The water molecules were constrained at their experimental geometry (r_{OH} = 0.9572 Å, $\angle_{HOH}$ = 104.52°[82]) whereas the geometries of the whole water hexamers were taken from ref 23.

TABLE 1: Symmetrically Equivalent Multimers within the Hexamer

multimer	rep.[a]	composition
monomers[b]	6	(1)
dimers	3	(1,2) (1,3) (1,4) (1,6) (2,4)
trimers	3	(1,2,3) (1,2,4) (1,2,5) (1,2,6) (1,3,6) (1,4,6)
	1	(1,3,5) (2,4,6)
tetramers	3	(1,2,3,4) (1,2,3,5) (1,2,3,6) (1,2,4,5) (1,2,4,6)
pentamers	3	(1,2,3,4,5) (1,2,3,4,6)
hexamers[c]	1	(1,2,3,4,5,6)

[a] Number of multimers replaced by C_3 symmetry operations. [b] No monomer relaxation. [c] Geometries taken from ref 23.

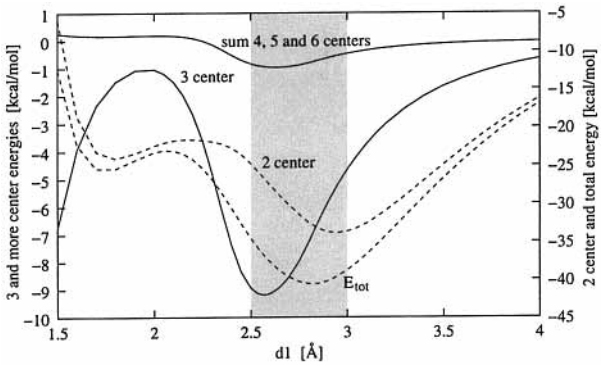

Figure 2. Many-body energies at the SCF level.

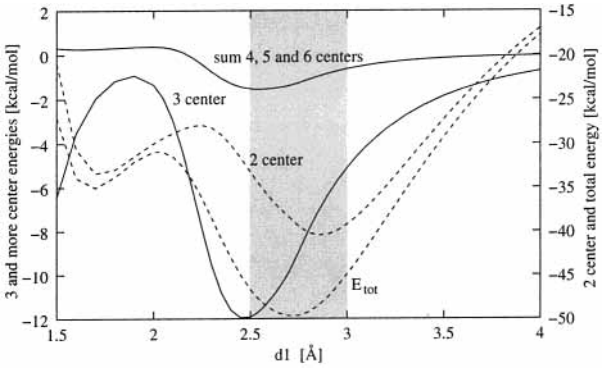

Figure 3. Many-body energies at the MP2 level.

The number of subsets T_M of size M from a cluster comprising N molecules ($N = 6$ for the hexamer) is given:

$$T_M = \binom{N}{M} = \frac{N!}{M!\,(N-M)!} \tag{3}$$

T_M increases rapidly with the size of the cluster as do the computational costs. These costs can be reduced by exploiting the symmetry of the cluster. Table 1 shows the results of this procedure for the hexamer (the numbers given in brackets refer to the individual water molecules in the hexamer as indicated in Figure 1b). The water hexamer under surface constraints has C_3 symmetry, which reduces the computational cost by roughly 60%.

In this communication we focus on the total binding energy E_{TOT} of the hexamer, and therefore from eq 1,

$$E_{TOT}(\mathbf{x}_1, ..., \mathbf{x}_N) = E_{ABS} - E_{1c} = E_{2c} + E_{3c} + ... + E_{Nc} \tag{4}$$

3. Results

Figures 2 and 3 display the composition of the interaction energy E_{TOT} according to eq 4. As observed previously,[23] the shape and curvature of the plots are independent of the level of computation, and the minima of the MP2 curves are shifted by about 0.1 Å toward smaller values of d1 in comparison with the SCF results. This shift can be explained as a consequence of the inclusion of electron correlation, which generally allows the nuclei of ground-state molecules to get closer to each other at correlated levels than at HF.

TABLE 2: Energies at the Global Minimum

	SCF	MP2
d1	2.80	2.70
r_{OO}	2.83	2.74
E_{TOT}	−40.588 (100%)	−49.667 (100%)
E_{2c}	−32.499 (80%)	−38.421 (77%)
E_{3c}	−7.275 (18%)	−9.858 (20%)
E_{4c}	−0.736 (2%)	−1.236 (2%)
E_{5c}	−0.073	−0.143
E_{6c}	−0.005	−0.010
E_{mc}[a]	−8.089 (20%)	−11.247 (23%)

[a] $E_{mc} = E_{3c} + E_{4c} + E_{5c} + E_{6c}$ distances in Å, energies in kcal mol^{-1}.

TABLE 3: Multicenter Energies in the Free Water Hexamer

	SCF	MP2
r_{OO}	2.83	2.73
E_{TOT}	−44.039 (100%)	−53.747 (100%)
E_{2c}	−35.045 (80%)	−41.395 (77%)
E_{3c}	−8.087 (18%)	−10.790 (20%)
E_{hc}[a]	−0.907 (2%)	−1.562 (3%)
E_{mc}[b]	−8.994 (20%)	−12.353 (23%)

[a] $E_{hc} = E_{4c} + E_{5c} + E_{6c}$. [b] $E_{mc} = E_{3c} + E_{4c} + E_{5c} + E_{6c}$ distances in Å, energies in kcal mol^{-1}.

At both levels of computation, multicenter energies contribute significantly to the total interaction energy E_{TOT} (up to 23% at the global minimum on MP2 level, Table 2). Despite the dominance of three-center energies, the four-center energies also contribute considerably to E_{TOT} (2% on both levels of theory). These results are in good agreement with those for the free hexamer (S_6 symmetry, Table 3). All significant energy contributions are scaled down by the same factor (SCF: 7.8%, MP2: 7.6%) and as the relative energy contributions do not change while the water hexamer binds to the virtual surface any substantial changes in the bonding mechanism can be ruled out.

Figures 2 and 3 demonstrate the strong influence of the multicenter energies on the geometry of the hexamer and hence on the structure of the bilayer as a function of surface lattice constant d1. The two-center energies have their minima close to the upper end of the experimentally observed region of surface lattice constants (SCF: 2.95 Å, MP2: 2.85 Å) whereas the three-center energies have their minima at the lower end (SCF: 2.58 Å, MP2: 2.45 Å). The combination of the two- and multicenter energy contributions, moves the minimum of E_{TOT} closer to the experimentally observed optimum for a water bilayer on a metal surface (RHF: 2.80 Å, MP2: 2.70 Å, Exp. 2.71 Å as the most stable water bilayer has been observed on Ru(0001)[5,23]), but not sufficiently to reach the idealized value of ice Ih (2.6 Å[23]).

Most multicenter energy curves show strong oscillations with a well defined maximum and minimum and a shallow second minimum. Table 4 summarizes the stationary points of the multicenter energy curves. The general agreement between SCF and MP2 results decreases as the order of the multicenter energies increases. This misalignment can be rationalized with the size of the energy contribution. As the order of the multicenter contributions increases their magnitude decreases rapidly (Tables 2 and 4), and differences in quality between

TABLE 4: Extrema of Multicenter Energies

	1. min. (SCF)		1. min. (MP2)		2. min. (SCF)		2. min. (MP2)		max. (SCF)		max. (MP2)	
centers	d1[a]	E_{ic}	d1[a]	E_{ic}	d1[a]	E_{ic}	d1[a]	E_{ic}	d1[a]	E_{ic}	d1[a]	E_{ic}
2	2.95	−33.851	2.85	−40.450	2.52	−25.300	1.70	−33.357	2.15	−21.634	2.25	−27.899
3	2.58	−9.189	2.45	−11.952					2.00	−1.040	1.90	−0.924
4	2.62	−0.885	2.52	−1.399	1.70	0.142	1.60	0.158	2.00	0.162	2.00	0.287
5	2.68	−0.083	2.62	−0.149	1.90	0.032	1.90	0.086	2.15	0.039	2.10	0.100
6	2.75	−0.005	2.70	−0.010	1.70	−0.003			2.40	0.003	2.30	0.012
sum	2.80	−40.588	2.70	−49.667	1.70	−25.415	1.70	−35.036	2.05	−23.026	2.00	−30.935

[a] Values for d1 taken from the corresponding energy curves: d1 is given in Å and energies E_{ic} in kcal mol^{-1}.

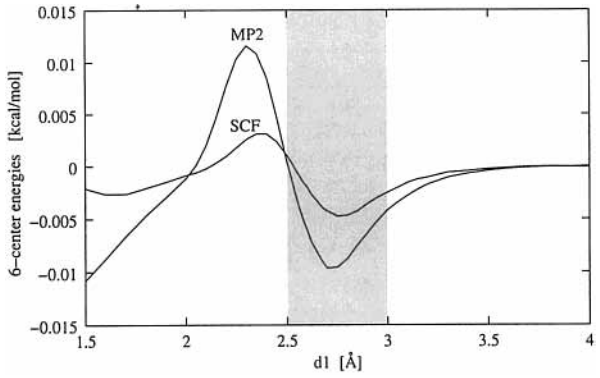

Figure 4. Six-center energies at the SCF and MP2 level.

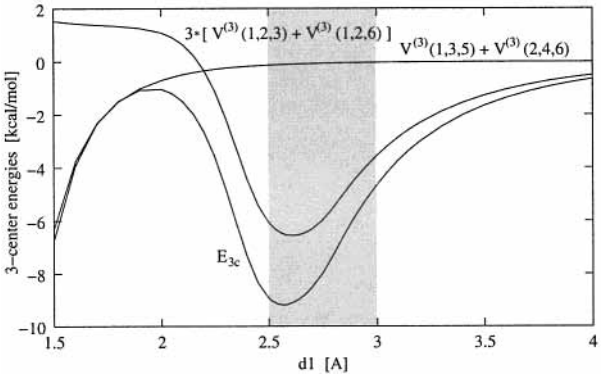

Figure 5. Three-body energies at the SCF level.

the levels of computation become more pronounced. The poorest alignment of SCF and MP2 results has been observed for E_{6c} (Figure 4). The shallow second minimum of the SCF curve is absent at the MP2 level. Due to this misalignment the calculations can only provide rough estimates for E_{6c} for d1 $\gtrsim$ 2 Å, indicating that the value for d1 at the six center energy minimum lies close to that for the minimum of E_{TOT}.

The shapes of the E_{3c} curves agree very well at SCF and MP2 levels, despite limitations of the model. Figures 2 and 3 show a well-defined minimum and maximum, but no second minimum. The three-center energies E_{3c} are bonding for all values of d1, while multicenter energies of orders higher than 3 become antibonding as d1 decreases.

Figures 5 and 6 show the composition of E_{3c} at SCF and MP2 levels. As electron correlation is included into the model, the three-center energies and their relative contribution to E_{TOT} increase, thus favoring a shorter oxygen−oxygen separation, which again results in smaller values for d1 at the global minimum of E_{3c}. As both figures are in reasonable agreement, this communication focuses just on the MP2 results for E_{3c}. Higher order many-body interaction energies will not be discussed in detail, since they contribute only little to E_{TOT} (Table 2).

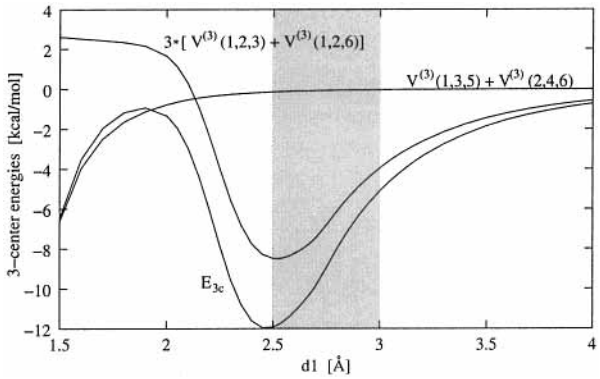

Figure 6. Three-body energies at the MP2 level.

Figure 6 displays the behavior of E_{3c} as a function of the surface lattice constant d1. In the experimentally observed region of surface lattice constants, three-center energies from direct neighbors E_{3c} ($V^{(3)}$(1, 2, 3) and $V^{(3)}$(1, 2, 6)) are dominant (the sum of both energies has to be multiplied by 3 to account for the symmetry of the hexamer). The sum of three-center energy contributions from directly bound water molecules has its minimum at 2.52 Å, close to that of E_{3c} (2.45 Å), and becomes increasingly antibonding as d1 decreases further.

It was shown previously,[23] that the hexamer splits into two trimers as d1 becomes very small. Each trimer is formed from the water molecules in the same layer. In agreement with this observation, E_{3c} is controlled by contributions from $V^{(3)}$(1, 3, 5) and $V^{(3)}$(2, 4, 6) at very small values of d1 (−6.6 kcal/mol for d1 = 1.5 Å). The effect of multicenter forces in cyclic water clusters is stronger than in linear water clusters, because all water molecules simultanously donate and receive electron density, thereby minimizing charge formation on the individual water molecules.[37,83−85] The three-center energies $V^{(3)}$(1, 3, 5) and $V^{(3)}$(2, 4, 6) decrease rapidly in size as d1 increases. At d1 = 2.13 Å, the curve for the energy contributions from the cyclic trimers crosses that for the energy contributions from the linear clusters (3[$V^{(3)}$(1, 2, 3) + $V^{(3)}$(1, 2, 6)], Figure 6). The maximum of E_{3c} can therefore be explained by a change in the dominance of the individual multicenter interactions $V^{(3)}$, especially since E_{3c} and the sum of both contributions to $V^{(3)}$ have their maximum at the same position (d1 = 1.9 Å).

4. Discussion

RHF and MP2 results (Table 2) for the multicenter energies differ by 3% at their global minima (RHF d1 = 2.8 Å, MP2 d1 = 2.7 Å) under surface constraints but are essentially in agreement: multicenter energies contribute significantly (MP2: 23%) to the total energy of the cluster and should therefore be considered explicitly in a valid model.

The total energy of the hexamer is reduced by 4.08 kcal mol^{-1} (MP2 level) on the virtual surface. The comparison (Tables 2 and 3) of the relative energy contributions to E_{TOT} shows that

TABLE 5: Interaction Energies in the Trimer

	linear trimer				cyclic trimer			
	Pot N	TIP4P	DZP/MP2	DZP/MP3	Pot N	TIP4P	DZP/MP2	DZP/MP3
r_{OO}[a]	2.9697	2.7342	2.8435	2.8687	2.9135	2.7689	2.7778	2.801
α[b]	5.8	0.5	2.7	1.6	24.2	15.7	23.6	23.54
E_{TOT}	−10.547	−13.314	−14.307	−11.085[c]	−13.685	−16.565	−17.020	−13.789[c]
$V^{(2)}$ (1, 2)	−4.891	−6.232	−6.232	−4.681[c]	−4.561	−5.522	−5.004	−3.644[c]
$V^{(2)}$ (1, 3)	−0.764	−0.849	−0.820	−0.729[c]	−4.561	−5.522	−5.004	−3.644[c]
$V^{(2)}$ (2, 3)	−4.891	−6.232	−6.232	−4.681[c]	−4.561	−5.522	−5.004	−3.644[c]
E_{2c}	−10.547	−13.314	−13.282	−10.091[c]	−13.685	−16.565	−15.011	−10.923[c]
E_{3c}			−1.025	−0.994[c]			−2.009	−2.866[c]

[a] Oxygen−oxygen distance in the cluster, given in Å. [b] Angle between the oxygen−oxygen bond and the bonding oxygen−hydrogen vector of the hydrogen donator, given in degrees. [c] BSSE corrected with the counterpoise method according to Boys and Bernadi;[91] Pot N from ref 23 and TIP4P from ref 90. All energies given in kcal mol^{-1}.

all energies are scaled down by the same factor upon adsorption onto the virtual surface and therefore can be compared with values published previously for the free hexamer.[59−63]

At the MP2 level multicenter energies contribute more (23%) to the total energy than at the SCF level (20%). This increase in multicenter energies can be explained by the more compact cluster geometry with shorter oxygen−oxygen distances at the MP2 level. Multicenter forces usually extend less far than the two-center ones. In a more compact cluster geometry arising from the inclusion of electron correlation, multicenter energies contribute more to E_{TOT} than in a loosely bound one. This effect has been previously reported for the free water hexamer by Kim et al.[63] The MP2 two-center energy contribution of 77% is large compared with values published previously (79%,[59] 77%,[60] 72%−73%,[61] 69%−75%,[62] 76%−78%[63]) and may be partially attributed to the rigid monomer geometries.[62] Consequently, the three-center contributions (20%) are smaller than published values (21%,[60] 23%−24%,[61] 21%−25%[62]) while again the value of the multicenter energies of higher order (3%) agree well with literature values (3%−4%[60−62]).

The close similarity of the relative energy contributions in the free and the surface constrained water hexamer suggests that the binding mechanisms within the clusters are essentialy the same for both. By construction of the model, the water−hexamer can be used to describe the water bilayer at the metal−water interface.[23] Saykally et al. pointed out that the free hexamer can be used as a first approximation to ice, since the oxygen−oxygen distance in the free hexamer (2.73 Å, Table 3) agrees well with that for ice (2.76 Å).[70] It is then possible to assume that the energetics in the bilayer are similar to those observed in ice.[23]

The strong influence of the three-center forces on the total energy at the MP2 level is shown in Table 4 and Figure 3. The global minimum of E_{3c} (2.45 Å, −11.9 kcal/mol, Table 4) is found at a smaller value for d1 than that expected for ice Ih (2.6 Å[23]). Figures 2 and 3 demonstrate how the multicenter energies, which are controlled by E_{3c}, force the global minimum of E_{TOT} into the experimentally observed region (SCF: d1 = 2.8 Å, MP2: d1 = 2.7 Å). This observation agrees well with results published by Yoon, Morokuma, and Davidson,[74] who assumed, that the multicenter energies governing the structure of ice are controlled by the contributions from direct neighbors. Consequently, their model potential for the anaylsis of the ice focused on a suitable description of $V^{(3)}$(1, 2, 3) and $V^{(3)}$(1, 2, 6). The authors of ref 74 were able show that the shorter hydrogen bond in ice (compared with that in the dimer) can be rationalized with the three-center energies arising from directly connected water molecules.

Our calculations as shown in Figure 6 verified this assumption for the hexamer on a virtual surface. The three-center forces are indeed controlled by $V^{(3)}$(1, 2, 3) and $V^{(3)}$(1, 2, 6), and as for the ice crystal, they create shorter hydrogen bonds in the bilayer structure than a simple two-center model suggests. Since the sum of $V^{(3)}$(1, 2, 3) and $V^{(3)}$(1, 2, 6) has its minimum (d1 = 2.52 Å) close to that of E_{3c} and is also similar in magnitude, it is then possible to assume that the properties of the bilayer structure are indeed controlled by three-center forces among directly connected water molecules.

The observation that multicenter energies in the bilayer are controlled by $V^{(3)}$(1, 2, 3) and $V^{(3)}$(1, 2, 6) can also be used to explain another result arising from simulations of the electrochemical metal−water interface. Berkowitz[86,87] and Spohr[20,21,88] published molecular dynamics simulations of the platinum−water interface using an effective water−water interaction potential. Saykally et al.[26] and Brodsky[89] pointed out that calculations for gas-phase water clusters with effective water−water interaction potentials are unreliable, since these potentials are not designed for this task. Many-body effects are included into the model by the parameterization of the potential energy functions. These parameters were designed to describe the bulk, in which an individual water molecule is evenly surrounded by its peers. At the electrochemical interface the water molecules in the bilayer are not evenly surrounded by other water molecules, and the application of effective water−water interaction potentials is therefore prone to failure.

The inclusion of many-body effects into effective pairwise potentials results generally in stronger hydrogen bonds and more attractive interactions between second next neighbors than accurate calculations on small water clusters or experimental data suggest.[85] These enforced interactions between second next neighbors can partially compensate for many-body effects in linear water clusters, but fail for compact, highly strained clusters.[85] In Table 5, data obtained with effective water−water interaction potentials (Pot N,[23] TIP4P[90]) for a linear (two ideal hydrogen bonds, all head−tail connected) and a cyclic (C_{3h} symmetry) trimer are compared with results from quantum chemical calcualtions (DZP/MP2 and DZP/MP3 with BSSE energy correction[91]). The three-center energies in the cyclic trimer are generally much stronger than in the linear trimer,[37] because only the central water molecule (number 2) in the linear trimer simultaneously donates and receives electron density, while in the cyclic one all three water molecules do so.[85] In the linear trimer, charges cumulate at the water molecules at the end of the chain ($|q|$ = 0.028 e on the MP3 level). The strong three-center bonds in the cyclic trimer can compensate for the distortion of the hydrogen bonds (at the MP3 level −3.64 kcal mol^{-1} in the trimer versus −4.91 kcal mol^{-1} in the dimer[23]) and so lower the total energy. The effective potentials cannot reproduce this effect satisfactorily. The values for E_{TOT} obtained with effective interaction potentials are close to the quantum

chemical values, because the individual hydrogen bonds are stronger than in quantum chemical calculations and generate large values for E_{2c}. On the other hand, the reproduction of the quantum chemical results for the linear trimer using effective interaction potentials was satisfactory, as three-center energies contribute less to E_{TOT} in the linear trimer than in the cyclic one. The stronger two-center bonds calculated with the effective interaction potentials can therefore compensate sufficiently for the missing three-center energy contribution, and the energy of formation E_{TOT} is well reproduced.

As the structure of the blilayer appears to be dominated by $V^{(3)}(1, 2, 3)$ and $V^{(3)}(1, 2, 6)$ (caused by linear trimer geometries), effective potentials such as TIP4P can be used to explore simultaneously both the bulk electrolyte and the interface, and results from these simulations can be related to those from UHV experiments.

The results at SCF and MP2 levels (Figures 2 and 3) suggest that cooperative effects have a significant influence on the value of the surface lattice constant d1 for the optimal growth of the bilayer. The three-center forces seem to favor metals with small values for d1, but they cannot compensate completely for the strong two-center energies, which seem to favor metals with large values of d1. This result is in agreement with other results reported for the surface of ice Ih.[92−94] Distortions of the hydrogen bonded network at the surface can cause instabilities at the surface resulting in an increase of the hydrogen bonds and can therefore lead to the formation of a liquid-like layer at the surface. This process is commonly known as surface premelting. Kroes[93] used for his studies the TIP4P calculation, whereas as Minot et al.[95] used ab initio calculations for their analysis. Both groups came to the same conclusion, namely that absent hydrogen bonds at the surface result in strong vibrational motions perpendicular to the surface, reducing the nonplanarity of the topmost bilayer in the ice crystal to a value close to zero. Our calculation,[23] on the other hand, showed that ring puckering and values for surface lattice constant close to that for bulk ice are energetically disfavored in the bilayer structure. The nonplanarity of the water hexamer observed in bulk ice Ih seems therefore to be the result of two effects: strong directional hydrogen bonds and a maximum in the three-center energies caused by direct neighbors ($V^{(3)}(1, 2, 3)$ and $V^{(3)}(1, 2, 6)$). The water bilayer on the metal surface, similar to that on an ice crystal, is in a different environment to that in bulk ice. One directional hydrogen bond is absent as is the direct neighbor for the three-center energies. With increasing values of water-coverage of the surface, more directional hydrogen bonds will be formed and also the number of directly connected water trimers within the water layers will increase. It seems justified to assume that, with increasing number of water layers, the properties of the multilayer will become similar to those of bulk ice, as suggested preveously by the analysis of the total energy.[23]

5. Conclusions

The calculations presented here demonstrate the importance of cooperative effects within the water layer for the structure of the metal−water interface, where the metal is represented by a set of geometrical contraints based on the value of the surface lattice constant (virtual surface). These effects can account for the special properties of the interface. Many-body effects support the formation of the water bilayer on metals with surface lattice constants within the experimentally observed region (2.49 Å ≤ d1 ≤ 2.89 Å), while models based on two-center forces tend to favor too large values for d1. Close inspection of the multicenter energies showed that cooperative effects are dominated by those originating from directly connected water trimers. As the effects of these forces are generally reasonably well described by effective water−water interaction potentials, the good results of models of the interface using effective water−water interaction potentials can be rationalized. As the number of directional hydrogen bonds in the bilayer is small, these three-center energies cannot force the bilayer into a geometry similar to that observed at the surface of bulk ice. The calculations reported here suggest that the structure of the bilayer is closer to that of the premolten water layer on an ice crystal than to that of bulk ice Ih.

Acknowledgment. T.L. would like to thank K. Nagorny in Hamburg (D) and I. L. Cooper in Newcastle upon Tyne (GB) for their support and the Job-Stiftung (D) for funding this work.

References and Notes

(1) Kua, J.; Goddard, W. A., III *J. Phys. Chem. B* **1998**, *102*, 9492−9500.
(2) Kua, J.; Goddard, W. A., III *J. Am. Chem. Soc.* **1999**, *121*, 10928−10941.
(3) Chang, S.-C.; Weaver, M. J. *J. Phys. Chem.* **1991**, *95*, 5391−5400.
(4) Kizhakevarim, N.; Jiang, X.; Weaver, M. J. *J. Chem. Phys.* **1994**, *100*, 6750−6764.
(5) Thiel, P. A.; Madey, T. E. *Surf. Sci. Rep.* **1987**, *7*, 211−385.
(6) Winter, M. WebElements Periodic Table URL http://www.webelements.com/
(7) Firment, L. E.; Somorjai, G. A. *Surf. Sci.* **1976**, *55*, 413−426.
(8) Firment, L. E.; Somorjai, G. A. *J. Chem. Phys.* **1975**, *63*, 1037−1038.
(9) Garwood, G. A., Jr.; Hubbard, A. T. *Surf. Sci.* **1982**, *118*, 223−247.
(10) Wagner, F. T.; Ross, P. N., Jr. *Surf. Sci.* **1985**, *160*, 305−330.
(11) Starke, U.; Matere, N.; Barbieri, A.; Döll, R.; Heinz, K.; Van Hove, M. A.; Somorjai, G. A. *Surf. Sci.* **1993**, *287/288*, 432−437.
(12) Madey, T. E.; Yates, J. T., Jr. *Chem. Phys. Lett.* **1977**, *51*, 77−83.
(13) Thiel, P. A.; Hoffmann, F. M.; Weinberg, W. H. *J. Chem. Phys.* **1981**, *75*, 5556−5572.
(14) Doering, D.; Madey, T. *Surf. Sci.* **1982**, *123*, 305−337.
(15) Bernal, J. D.; Fowler, R. H. *J. Chem. Phys.* **1933**, *1*, 515−546.
(16) Pauling, L. *J. Am. Chem. Soc.* **1935**, *57*, 2680−2684.
(17) Pauling, L. *General Chemistry*, 3rd ed.; W. H. Freeman & Co.: San Francisco, 1970.
(18) Schulson, E. M. *JOM* **1999**, *51*, 21−27. URL http://www.tms.org/pub/journals/JOM/9902/Schulson-9902.html.
(19) Lankau, T.; Nagorny, K.; Cooper, I. L. *Langmuir* **1999**, *15*, 7308−7315.
(20) Spohr, E.; Heinzinger, K. *Ber. Bunsen-Ges. Phys. Chem.* **1988**, *92*, 1358−1363.
(21) Spohr, E. *J. Phys. Chem.* **1993**, *93*, 6171−6180.
(22) Spohr, E.; *Computer Modelling of Aqueous/Metallic Interfaces*; Habilitation's thesis; University of Ulm, 1995.
(23) Lankau, T.; Cooper, I. L. *J. Phys. Chem. A* **2001**, *105*, 4084−4095.
(24) Burke, L. A.; Jensen, J. O.; Jensen, J. L.; Krishnan, P. N. *Chem. Phys. Lett.* **1993**, *206*, 293−296.
(25) Lentz, B. R.; Scheraga, H. A. *J. Chem. Phys.* **1973**, *58*, 5296−5308.
(26) Liu, K.; Cruzan, J. D.; Saykally, R. J. *Science* **1996**, *271*, 929−933.
(27) Brown, M. G.; Keutsch, F. N.; Saykally, R. J. *J. Chem. Phys.* **1998**, *109*, 9645−9647.
(28) Cruzan, J. D.; Braly, L. B.; Liu, K.; Brown, M. G.; Saykally, R. J. *Science* **1996**, *271*, 59−62.
(29) Liu, K.; Brown, M. G.; Saykally, J. R. *Science* **1996**, *271*, 62−64.
(30) Loerting, T.; Liedl, K. R.; Rode, B. M. *J. Chem. Phys.* **1998**, *109*, 2672−2679.
(31) Corrales, L. R. *J. Chem. Phys.* **1999**, *110*, 9071−9080.
(32) Merrill, G. N.; Gordon, M. S. *J. Phys. Chem. A* **1998**, *102*, 2650−2657.
(33) Wales, D. J.; Walsh, T. R. *J. Chem. Phys.* **1997**, *106*, 7193−7207.
(34) Xantheas, S. S. *NATO ASI series C* **2000**, *561*, 119−128.
(35) Xantheas, S. S.; Dunning, T. H., Jr. *J. Chem. Phys.* **1993**, *99*, 8774−8792.
(36) Gregory, J. K.; Clary, D. C. *J. Phys. Chem.* **1996**, *100*, 18014−18022.
(37) Ludwig, R. *Angew. Chem., Int. Ed.* **2001**, *40*, 1808−1827.
(38) Jensen, J. O.; Burke, L. A.; Krishnan, P. N. *Chem. Phys. Lett.* **1995**, *241*, 253−260.

(39) Jensen, J. O.; Krishnan, P. N.; Burke, L. A. *Chem. Phys. Lett.* **1995**, *246*, 13−19.
(40) Rodriguez, J.; Laria, D.; Marceca, E. J.; Estrin, D. A. *J. Chem. Phys.* **1999**, *110*, 9039−9047.
(41) Brudermann, J.; Melzer, M.; Buck, U.; Kazimirzki, J. K.; Sadlej, J.; Bush, V. *J. Chem. Phys.* **1999**, *110*, 10649−10652.
(42) Buck, U.; Ettischer, I.; Melzer, M.; Bush, V.; Sadlej, J. *Phys. Rev. Lett.* **1998**, *80*, 2578−2581.
(43) Jiang, J. C.; Chang, J.-C.; Wang, B.-C.; Lin, S. H.; Lee, Y. T.; Chang, H.-C. *Chem. Phys. Lett.* **1998**, *289*, 373−382.
(44) Nigra, P.; Kais, S. *Chem. Phys. Lett.* **1999**, *305*, 433−438.
(45) McDonald, S.; Ojamäe, L.; Singer, S. J. *J. Phys. Chem. A* **1998**, *102*, 2824−2831.
(46) Burnham, C. J.; Li, J.; Xantheas, S. S.; Leslie, M. *J. Chem. Phys.* **1999**, *110*, 4566−4581.
(47) Kim, J.; Majumdar, D.; Lee, H. M.; Kim, K. S. *J. Chem. Phys.* **1999**, *110*, 9128−9134.
(48) Wales, D. J.; Hodges, M. P. *Chem. Phys. Lett.* **1998**, *286*, 65−72.
(49) Laasonen, K.; Parinello, M.; Car, R.; Lee, C.; Vanderbilt, D. *Chem. Phys. Lett.* **1993**, *207*, 208−213.
(50) Franken, K. A.; Jalaie, M.; Dykstra, C. E. *Chem. Phys. Lett.* **1992**, *198*, 59−66.
(51) Lee, C.; Chen, H.; Fitzgerald, G. *J. Chem. Phys.* **1994**, *101*, 4472−4473.
(52) Krishnan, P. N.; Jensen, J. O.; Burke, L. A. *Chem. Phys. Lett.* **1994**, *217*, 311−318.
(53) Gregory, J. K.; Clary, D. C.; Liu, K.; Brown, M. G.; Saykally, R. J. *Science* **1997**, *275*, 814−817.
(54) Kryachko, E. S. *Chem. Phys. Lett.* **1999**, *314*, 353−363.
(55) Xantheas, S. S. *J. Chem. Phys.* **1995**, *102*, 4505−4517.
(56) Kim, J.; Kim, K. S. *J. Chem. Phys.* **1998**, *109*, 5886−5895.
(57) Mhin, B. J.; Kim, H. S.; Kim, H. S.; Yoon, C. W.; Kim, K. S. *Chem. Phys. Lett.* **1991**, *176*, 41−45.
(58) Tsai, C. J.; Jordan, K. D. *Chem. Phys. Lett.* **1993**, *213*, 181−188.
(59) Kim, K. S.; Dupuis, M.; Lie, G. C.; Clementi, E. *Chem. Phys. Lett.* **1986**, *131*, 451−456.
(60) Xantheas, S. S. *J. Chem. Phys.* **1994**, *100*, 7523−7534.
(61) Pedulla, J. M.; Jordan, K. D. *NATO ASI series C* **2000**, *561*, 35−44.
(62) Pedulla, J. M.; Kim, K.; Jordan, K. D. *Chem. Phys. Lett.* **1998**, *291*, 78−84.
(63) Mhin, B. J.; Kim, J.; Lee, S.; Lee, J. Y.; Kim, K. S. *J. Chem. Phys.* **1993**, *100*, 4484−4486.
(64) Clary, D. C.; Gregory, J. K. *NATO ASI series C* **2000**, *561*, 187−200.
(65) Kim, K.; Jordan, K. D.; Zwier, T. S. *J. Am. Chem. Soc.* **1994**, *116*, 11568−11569.
(66) Kim, K. S.; Kim, J. *NATO ASI series C* **2000**, *561*, 109−117.
(67) Tissandier, M. D.; Singer, S. J.; Coe, J. V. *J. Phys. Chem. A* **2000**, *104*, 752−757.
(68) Gregory, J. K.; Clary, D. C. *J. Phys. Chem. A* **1997**, *101*, 6813−6819.
(69) Liu, K.; Brown, M. G.; Carter, C.; Saycally, R. J.; Gregory, J. K.; Clary, D. C. *Nature (London)* **1996**, *381*, 501−503.
(70) Liu, K.; Brown, M. G.; Saykally, J. R. *J. Phys. Chem. A* **1997**, *101*, 8995−9010.
(71) Severson, M. W.; Buch, V. *J. Chem. Phys.* **1999**, *111*, 10866−10875.
(72) Nauta, K.; Miller, R. E. *Science* **2000**, *287*, 293−295.
(73) Fajardo, M. E.; Tam, S. *J. Chem. Phys.* **2001**, *115*, 6807−6810.
(74) Yoon, B. J.; Morokuma, K.; Davidson, E. R. *J. Chem. Phys.* **1985**, *83*, 1223−1231.
(75) Belford, D.; Campbell, E. S. *J. Chem. Phys.* **1984**, *80*, 3288−3296.
(76) Berendsen, H. J. C.; Grigera, J. R.; Straatsma, T. P. *J. Phys. Chem.* **1987**, *91*, 6269−6271.
(77) Hankins, D.; Moskowitz, J. W.; Stillinger, F. H. *J. Chem. Phys.* **1970**, *53*, 4544−4554.
(78) Xantheas, S. S. *Philos. Mag. B* **1996**, *73*, 107−115.
(79) Hodges, M. P.; Stone, A. J.; Xantheas, S. S. *J. Phys. Chem. A* **1997**, *101*, 9163−9168.
(80) Frisch, M. J.; Trucks, G. W.; Schlegel, H. B.; Gill, P. M. W.; Johnson, B. G.; Robb, M. A.; Cheeseman, J. R.; Keith, T.; Petersson, G. A.; Montgomery, J. A.; Raghavachari, K.; Al-Laham, M. A.; Zakrzewski, V. G.; Ortiz, J. V.; Foresman, J. B.; Cioslowski, J.; Stefanov, B. B.; Nanayakkara, A.; Challacombe, M.; Peng, C. Y.; Ayala, P. Y.; Chen, W.; Wong, M. W.; Andres, J. L.; Replogle, E. S.; Gomperts, R.; Martin, R. L.; Fox, D. J.; Binkley, J. S.; Defrees, D. J.; Baker, J.; Stewart, J. P.; Head-Gordon, M.; Gonzalez, C.; Pople, J. A. *Gaussian 94*, Revision C.2; Gaussian, Inc.: Pittsburgh, PA, 1995.
(81) Dunning, T. H., Jr. *J. Chem. Phys.* **1970**, *53*, 2823−2833.
(82) Benedict, W. S.; Gailar, N.; Plyer, E. K. *J. Chem. Phys.* **1956**, *24*, 1139−1165.
(83) Del Bene, J.; Pople, J. A. *J. Chem. Phys.* **1970**, *52*, 4858−4866.
(84) Mó, O.; Yáñez, M.; Elguero, J. *J. Chem. Phys.* **1992**, *97*, 6628−6638.
(85) Lankau, T. *A Computational Analysis of the Platinum-Water-Vacuum Interface*; Ph.D. Thesis; University of Hamburg, 2000. URL http://www.sub.uni-hamburg.de/disse/398/Diss.pdf
(86) Foster, K.; Raghavan, K.; Berkowitz, M. *Chem. Phys. Lett.* **1989**, *162*, 32−38.
(87) Raghavan, K.; Foster, K.; Motakabbir, K.; Berkowitz, M. *J. Chem. Phys.* **1991**, *94*, 2110−2117.
(88) Heinzinger, K.; Spohr, E. *Electrochim. Acta* **1989**, *34*, 1849−1856.
(89) Brodsky, A. *Chem. Phys. Lett.* **1996**, *261*, 563−568.
(90) Jorgensen, W. L.; Chandrasekhar, J.; Madura, J. D.; Impey, R. W.; Klein, M. L. *J. Chem. Phys.* **1983**, *79*, 926−935.
(91) Boys, S. F.; Bernardi, F. *Mol. Phys.* **1970**, *19*, 553−566.
(92) Dosch, H.; Lied, A.; Bilgram, J. H. *Surf. Sci.* **1995**, *327*, 145−164.
(93) Kroes, G.-J. *Surf. Sci.* **1992**, *275*, 365−382.
(94) Materer, N.; Starke, U.; Barbieri, A.; Van Hove, M. A.; Somorjai, G. A.; Kroes, G.-J.; Minot, C. *J. Phys. Chem.* **1995**, *99*, 6267−6269.
(95) Matsuoka, O.; Clementi, E.; Yoshimine, M. *J. Chem. Phys.* **1976**, *64*, 1351−1361.